Molecular Simulation of Permeation of Small Penetrants through Membranes. 2. Solubilities

Yoshinori Tamai,* Hideki Tanaka, and Koichiro Nakanishi

Department of Polymer Chemistry, Kyoto University, Kyoto 606-01, Japan

Received September 7, 1994; Revised Manuscript Received January 3, 1995[⊗]

ABSTRACT: The excess chemical potentials of methane, water, and ethanol in poly(dimethylsiloxane) (PDMS) and polyethylene (PE) were calculated by the Widom method. The excess chemical potentials of water and ethanol in aqueous ethanol solutions (0, 50, 100 wt %) were also calculated by the Shing−Gubbins method. The excluded volume map sampling (EVMS) method and the continuum configurational bias (CCB) method were used to increase the efficiency of sampling. In spite of the polarity and the internal degrees of freedom of the molecules, the excess chemical potentials could be calculated with a small statistical error. The solubilities of methane, water, and ethanol in the polymers were calculated from excess chemical potentials. Permeation rates calculated from diffusion coefficients and solubilities were in reasonable agreement with experimental data. The free volume cluster of each system was analyzed and was related to the permeation of small penetrants in the membranes.

Introduction

Poly(dimethylsiloxane) (PDMS) is used for ethanol permselective membranes in the separation of aqueous ethanol solution by pervaporation. Pervaporation[1] is a method for separating a mixture of liquids by membranes. The components of the liquid mixture are supplied on the feed side of the membrane and diffuse to the permeate side of the membrane, where the pressure is diminished, leaving the membrane as vapor. The separation process is accounted for by the sorption−diffusion model. The permeation rate P of small penetrants is expressed by

$$P = DS \tag{1}$$

where D is the diffusion coefficient and S is the solubility of each penetrant. The ratio of the permeation rates of each component leads to the separation factor. The separation factor can be predicted from solubilities and diffusion coefficients calculated by the molecular simulation technique.

We have already studied the diffusion process of methane, water, and ethanol in PDMS and in polyethylene (PE) by molecular dynamics (MD) simulations and obtained diffusion coefficients which agree reasonably with those from experiments.[2] In this paper, we consider the solubilities of small penetrants by molecular simulation techniques.

On the surface of membranes, the polymer/penetrant system is in equilibrium with the gas phase (in the case of gas separation) or the liquid phase (in the case of liquid separation such as pervaporation). The solubility of a small penetrant depends on the difference in chemical potentials between two phases. Excess chemical potentials can be calculated by the Widom test particle insertion method.[4] Alternatively, the phase equilibrium can be simulated directly by the Gibbs ensemble method.[5] These methods have been applied mainly to Lennard-Jones fluids. Nowadays, the Widom method is applicable also to polymer/penetrant systems. Müller-Plathe[6] calculated the excess chemical potentials of helium, hydrogen, nitrogen, oxygen, and methane in amorphous atactic polypropylene (a-PP). Sok et al.[7] calculated those of methane in PDMS, and Müller-Plathe et al.[8] those of methane, hydrogen, and oxygen in polyisobutylene (PIB). In those studies, the excess chemical potentials are overestimated compared with the experimental data. The excess chemical potential of small molecules in PIB which Gusev and Suter[9] calculated by the mean-field method was also overestimated. Müller-Plathe et al.[8] commented that these deviations could not be accounted for by incompleteness of the potential functions. They pointed out that the deviations could be caused by the nonuniformity of the amorphous polymer structure in the simulation; a small number of large holes exist in the starting structure and do not relax during the simulation time.

Thus far studies for polymer/penetrant systems have treated the excess chemical potential of small nonpolar molecules (mono-atomic or di-atomic). In this study, we consider polar molecules (water and ethanol) and a molecule which has internal degrees of freedom (ethanol). In these cases, it is difficult to obtain the excess chemical potentials with a certain precision. The Widom method needs to be combined with methods which raise the sampling efficiency. The excluded volume map sampling (EVMS) method,[10] in which no trial insertion is attempted in the region in which matrix atoms exist, has been generally used to increase the efficiency of sampling. For large molecules, we can raise the efficiency by biasing the orientation and the dihedral angles of a test molecule. Cracknell et al.[11] simulated the liquid−vapor equilibrium of water by the grand canonical ensemble Monte Carlo (MC) method and by the Gibbs ensemble method. The rotational insertion bias (RIB) method which biases the orientation of a trial insertion was used in their study. It was shown that the acceptance rate was increased by a factor of two. Using the continuum configurational bias (CCB) method, which biases the dihedral angles of an inserted molecule, de Pablo et al.[12] calculated the chemical potentials of linear hydrocarbons of carbon numbers up to 15 by the Widom method. Laso et al.[13] applied the method to the Gibbs ensemble simulation and examined phase equilibria of hydrocarbons.

Kumar et al.[14] applied an alternative method in which the chemical potential of a segment was calculated. The segmental chemical potential did not depend on the chain length for a long chain polymer which could be

[⊗] Abstract published in *Advance ACS Abstracts,* February 15, 1995.

0024-9297/95/2228-2544$09.00/0

treated as the Gaussian chain. Sheng et al.[15] studied phase equilibria of polymer systems with this method, and Kumar[16] considered polymer blend systems. This method, cannot be applied to short chain molecules because the segmental chemical potentials depend strongly on the chain length for these systems.

In this study, the excess chemical potentials of methane, water, and ethanol in PDMS and PE and those in aqueous ethanol solutions (0, 50, 100 wt %) are calculated by the Widom test particle insertion method and are compared to those by the Shing–Gubbins method.[17,18] The solubility of small molecules in the polymers has a simple relation to the excess chemical potential. The permeation rates of the small molecules in the polymers are calculated from the diffusion coefficients and the solubilities. A cluster analysis of the free volume is also made in order to establish a relation between the free volume and the solubility of a small molecule.

Model and Simulation Details

Programs and Potential Functions. All calculations were performed on CRAY Y-MP2E supercomputer using the molecular simulation program PAMPS which we coded. The AMBER/OPLS[19] force field was used except for PDMS and water. The GROMOS[7] force field was used for PDMS, and the SPC/E[20] for water. All CH_4, CH_3-, and $-CH_2-$ groups are treated as united atoms. A detailed description of the potential functions, generation of initial structures, and the MD simulations are given elsewhere.[2]

MD Simulation. The structures of amorphous PDMS and PE were generated in our previous paper.[2] The PDMS and PE samples are modeled as $CH_3[-Si(CH_3)_2O-]_{30}Si(CH_3)_3$ and $CH_3[-CH_2-]_{120}CH_3$, respectively. Simulations were carried out for systems containing five polymer chains in a cubic periodic box at the following experimental densities: 0.95 g/cm^3 for PDMS and 0.855 g/cm^3 for PE. The MD simulations were performed at 300 K under constant *NVE* conditions.

The simulations for aqueous ethanol solutions (0, 50, 100 wt %) were carried out under constant *NPT* conditions using the Nosé–Andersen method.[21,22] The iterative method of Ferrario and Ryckaert[23] was used to integrate the equations of motion with the Verlet algorithm and the SHAKE algorithm. The pressure was calculated from the atomic virial. The volume scaling was performed by atomic basis. The Lennard-Jones interactions were cut off at r_{cut} = 10 Å. The contributions to the pressure and the potential energy from the long tail of the pair potential were estimated by assuming that the radial distribution function $g(r)$ is unity for $r > r_{cut}$.[24] The Ewald sum was used for the calculation of the Coulombic interaction. The MD simulations were performed for aqueous ethanol solutions whose concentrations were 0 wt % (328 water molecules), 50 wt % (164 water molecules and 64 ethanol molecules), and 100 wt % (128 ethanol molecules). All the bond lengths and the bond angles were kept constant by the SHAKE algorithm. A time step of 0.5 fs was used. The molecules were confined in a cubic periodic box whose size was determined from the experimental density. After a steepest descent energy minimization, MD simulations were performed at 0.1 MPa and 300 K. After the systems were equilibrated, a trajectory of 100 ps was sampled for each system. The average unit cell lengths were 21.44, 22.35, and 23.52 Å for 0, 50, and 100 wt % solutions, respectively.

Particle Insertion Method. In the Widom method, insertion trials of test molecules were attempted for the systems which were obtained from the MD simulations. The excess chemical potential μ_r was calculated as

$$\mu_r = -kT \ln\langle \exp(-\psi/kT)\rangle_N \tag{2}$$

where ψ is the potential energy of the inserted (ghost) molecule with surrounding real molecules, and $\langle ... \rangle_N$ denotes the ensemble average over N molecules of the host matrix. For the *NPT* ensemble, eq 2 is replaced by

$$\mu_r = -kT \ln\left[\frac{\langle V \exp(-\psi/kT)\rangle_{NPT}}{\langle V\rangle_{NPT}}\right] \tag{3}$$

All the interactions were calculated in the same way as in the MD simulations. The interaction between a ghost molecule and its image was not included in the calculation. This is the situation in which a ghost molecule is inserted into a infinitely spreading matrix.

The EVMS (excluded volume map sampling) method[10] was used to increase the efficiency of sampling. For aspherical molecules, such as water and ethanol, an excluded volume map was constructed for the oxygen atom. The unit cell was divided into 100 × 100 × 100 grid points. If a grid point located at $\mathbf{r}_t$ satisfies the condition

$$|\mathbf{r}_t - \mathbf{r}_i| \le a\sigma_{ti} \tag{4}$$

where $\mathbf{r}_i$ is the position of a host atom i, σ_{ti} is the Lennard-Jones size parameter between the atoms t and i, and a is an empirical parameter, the grid point belongs to a family of excluded volume. Since the Boltzmann factor of the ghost molecule is approximately zero in the excluded volume, the insertion trials were attempted only at the grid points which are out of the excluded volume; the Boltzmann factor is multiplied by the weight, f_v/N_s, where f_v is a nonexcluded volume fraction and N_s is the number of samples for this configuration. We tested several values of the empirical parameters a and determined suitable values for a by referring to the energy distribution functions. The larger the value of a, the more the regions are excluded, and the greater the efficiency of EVMS. If the value a is too large, low-energy regions are also excluded and the calculated value of μ_r is estimated erroneously by EVMS. In the case of a = 1.0, the absolute value of μ_r is obviously underestimated by EVMS. For $a \le 0.9$, μ_r is independent of a. In this study we used a = 0.8 for all systems.

In the insertion of chain molecules, the CCB (continuum configurational bias) method[12] was used in combination with the EVMS method to increase the efficiency of the dihedral angle sampling. In this method, the chain of a test molecule is grown site by site in a way similar to the modified self-avoiding random walk method which was used for the generation of the initial structure of the polymers.[2] A dihedral angle is chosen among n_{dis} discretized points, which are equally spaced, with the probability

$$W_j = \frac{w_j}{\sum_{k=1}^{n_{dis}} w_k} \tag{5}$$

where w_j is the Boltzmann factor $\exp(-U_j/kT)$ for the jth discretized position of the dihedral angle. U_j is the interaction energy of the adding position j, which interacts with the atoms in the host matrix and also with the atoms in the already inserted part of the ghost molecule. The dihedral angle $[-\pi, \pi]$ is discretized into n_{dis} equally spaced values, the first of which is chosen at random. The excess chemical potential is calculated as

$$\mu_r = -kT \ln\langle W^{(m)} \exp(-\psi/kT)\rangle_N \tag{6}$$

where

$$W^{(m)} = \prod_{l=1}^{m} \left(\frac{1}{W_{j(l)} n_{dis}}\right) \tag{7}$$

where m is the number of dihedral angles in a ghost chain and $W_{j(l)}$ is equal to the value of W_j (eq 5) when the position of the lth dihedral angle is j. ψ is the potential energy of the inserted ghost molecule which has a set of dihedral angles, $[j(1), j(2), ..., j(m)]$. For ethanol, the insertion trial of the head group, H−O−CH_2−, was made with a random orientation, applying the EVMS method for the oxygen atom, and subsequently the $-CH_3$ group is inserted by the CCB method. The number of discretization of the dihedral angle n_{dis} was 12 in our calculations.

Shing−Gubbins Method. The ghost molecule energy distribution function

$$f(U) = \frac{\int \delta(\psi - U) \exp(-\Psi/kT)\, d\mathbf{q}_0\, d\mathbf{q}_1 \ldots d\mathbf{q}_N}{\int \exp(-\Psi/kT)\, d\mathbf{q}_1 \ldots d\mathbf{q}_N} \tag{8}$$

was calculated by the Widom method, where $\mathbf{q}_i$ is the coordinate of the ith molecule, including the coordinate of the center of mass, the orientation, and the internal degrees of freedom of the molecule. The coordinate of the test molecule is denoted by $\mathbf{q}_0$. $\Psi = \Psi(\mathbf{q}_1, \mathbf{q}_2, ..., \mathbf{q}_N)$ is the total potential of the N molecules system, $\psi = \psi(\mathbf{q}_0; \mathbf{q}_1, \mathbf{q}_2, ..., \mathbf{q}_N)$ is the potential of the inserted molecule with all other molecules, and δ is the Dirac delta function. The ensemble average is taken for the N host molecules. The value $f(U)\, dU$ is the probability that the interaction energy between the test (ghost) molecule and the host molecules lies in the range U to $U + dU$.

The real molecule energy distribution function

$$g(U) = \frac{\int \delta(\psi - U) \exp(-\psi/kT) \exp(-\Psi/kT)\, d\mathbf{q}_0\, d\mathbf{q}_1 \ldots d\mathbf{q}_N}{\int \exp(-\psi/kT) \exp(-\Psi/kT)\, d\mathbf{q}_0\, d\mathbf{q}_1 \ldots d\mathbf{q}_N} \tag{9}$$

was also calculated by the inverse-Widom method.[17,18] The ensemble average is taken for the $N + 1$ molecules including the test (real) molecule. The value $g(U)\, dU$ is the probability that the interaction energy between the test (real) molecule and the host molecules is in the range U to $U + dU$.

The ratio of eq 8 and eq 9 leads to

$$\ln [f(U)/g(U)] = U/kT - \mu_r/kT \tag{10}$$

This implies that a plot of $\ln[f(U)/g(U)]$ versus U has a slope of $1/kT$ and an intersection with the zero-energy axis of $-\mu_r/kT$.[17,18]

Solubility in Polymer. The solubility of a small penetrant in the ideal gas phase is calculated by

$$S_g = \exp(-\mu_r/RT) \tag{11}$$

where the solubility S is defined as the ratio of the number densities between two phases. The solubility of a small penetrant in the liquid phase is calculated by

$$S_l = \exp(-\Delta\mu_r/RT) \tag{12}$$

where $\Delta\mu_r = \mu_r^p - \mu_r^l$, and μ_r^p and μ_r^l are the excess chemical potentials in a polymer and in a liquid, respectively. In this study, we ignore any structural change which may occur in the membrane from the absorption of small penetrants.

Cluster Analysis of Free Volume. Arizzi et al.,[25] Greenfield and Theodorou,[26] and Misra and Mattice[27] made a cluster analysis of the free volume in polymers. We used a method similar to that of Misra and Mattice. The unit cell was divided into $100 \times 100 \times 100$ grid points on which a probe atom is settled. We selected the grid points (denoted by t) which satisfy the equation for all host atoms (denoted by i)

$$|\mathbf{r}_t - \mathbf{r}_i| \geq \frac{\sigma_t + \sigma_i}{2} \tag{13}$$

where $\mathbf{r}_t$ is the position of the test atom on the grid point, $\mathbf{r}_i$ is the position of the ith host atom, and σ_t and σ_i are the Lennard-Jones size parameters of the test atom t and the ith host atom. With this procedure, we can determine the grid points on which the probe atom can be settled without severe overlaps with the host atoms. The cluster analysis was performed for the accessible cubes whose centers are on the accessible grid points and whose edge lengths are equal to $^1/_{100}$th of the unit cell length. Assuming that the two accessible cubes which share a surface belong to the same cluster, the clusters of accessible cubes are constructed.

The cluster shape was also analyzed. Using the coordinates of the grid points which belong to the same cluster, we calculated a radius of gyration matrix $\mathbf{S}$. The elements of $\mathbf{S}$ are

$$S_{xx} = \sum_{i=1}^{N_g} x_i x_i$$

$$S_{xy} = \sum_{i=1}^{N_g} x_i y_i \tag{14}$$

$$\vdots$$

where N_g is the number of grid points in the cluster and (x_i, y_i, z_i) are the coordinates of the grid point relative to the center of the cluster. The eigenvalues of $\mathbf{S}$ are determined such that

$$X^2 \geq Y^2 \geq Z^2 \tag{15}$$

The squared radius of gyration s_j^2 and asphericity $(b/s^2)_j$ of cluster j are calculated from the eigenvalues:

$$s_j^2 = X^2 + Y^2 + Z^2 \tag{16}$$

$$(b/s^2)_j = \frac{X^2 - \frac{1}{2}(Y^2 + Z^2)}{X^2 + Y^2 + Z^2} \quad (17)$$

For clusters which contain only one accessible grid point, we define $s_j^2 = 0$ and $(b/s^2)_j = 0$. For each system, these values are calculated from 100 coordinates, averaged as

$$\langle A \rangle = \frac{\sum_{i=1}^{N_c} V_i A_i}{\sum_{i=1}^{N_c} V_i} \quad (18)$$

where A_i is an arbitrary quantity and V_i is the volume of the ith cluster. N_c is the total number of clusters which are contained in all the coordinates used for the calculation.

Results and Discussion

Simulation of Aqueous Ethanol Solution. The MD simulations were performed for the aqueous ethanol solutions (0, 50, 100 wt %) under constant *NPT* conditions. Phase separation was not observed for the ethanol 50 wt % solution; ethanol mixed with water uniformly.

Table 1 lists the densities and diffusion coefficients calculated from the MD simulations. The density of pure water agrees well with the experimental data. The densities of pure ethanol and 50 wt % ethanol solution are approximately 4% smaller than the experimental data. Jorgensen[28] simulated pure liquid ethanol by the *NPT* Monte Carlo method using the OPLS potential. He obtained a density of 0.748 ± 0.003 g/cm^3, which agrees with our value. The diffusion coefficients of pure water and ethanol agree well with the experimental values. The diffusion coefficients which are calculated from the MD simulation under the constant *NVT* conditions at the experimental densities are 2.38×10^{-5} and 1.11×10^{-5} cm^2/s,[2] which are almost the same as the values from the *NPT* simulations. The difference in density (4%) leads to the difference in the diffusion coefficient. In the 50 wt % aqueous ethanol solution, the diffusion coefficient of ethanol is smaller than that in the pure liquid.

Ghost Molecule Energy Distribution Function. The ghost molecule energy distribution function $f(U)$ was calculated by the Widom method. For the polymer/penetrant systems, 1000 coordinates were used as host matrices, and 10 000 insertion trials were performed for each coordinate. For the systems of the aqueous ethanol solutions (0, 50, 100 wt %), 10 000 coordinates were used as host matrices, and 1000 insertion trials were performed for each coordinate.

Figure 1a shows the $f(U)$ of water and ethanol in the aqueous ethanol solutions. Figures 2a and 3a show the $f(U)$ of methane, water, and ethanol in PDMS and in PE, respectively. Since the raw histograms of $f(U)$ fluctuate greatly in low-energy regions, the distribution functions were smoothed by the running average method in which an average value of the successive three columns of the histogram is put into the central column. This operation was applied to all columns, shifting the columns sequentially. The procedure was repeated three times to get the distribution functions shown in the figures.

Table 1. Densities and Diffusion Coefficients of Aqueous Ethanol Solutions

		$10^5 D$ (cm^2/s)	
c (wt %)	ϱ (g/cm^3)	ethanol	water
	Calculated		
0	0.995		2.63
50	0.878	0.71	1.62
100	0.752	1.21	
	Experimental[a]		
0	0.9965		2.14
50	0.91		
100	0.7851	1.01	

[a] From references in ref 2.

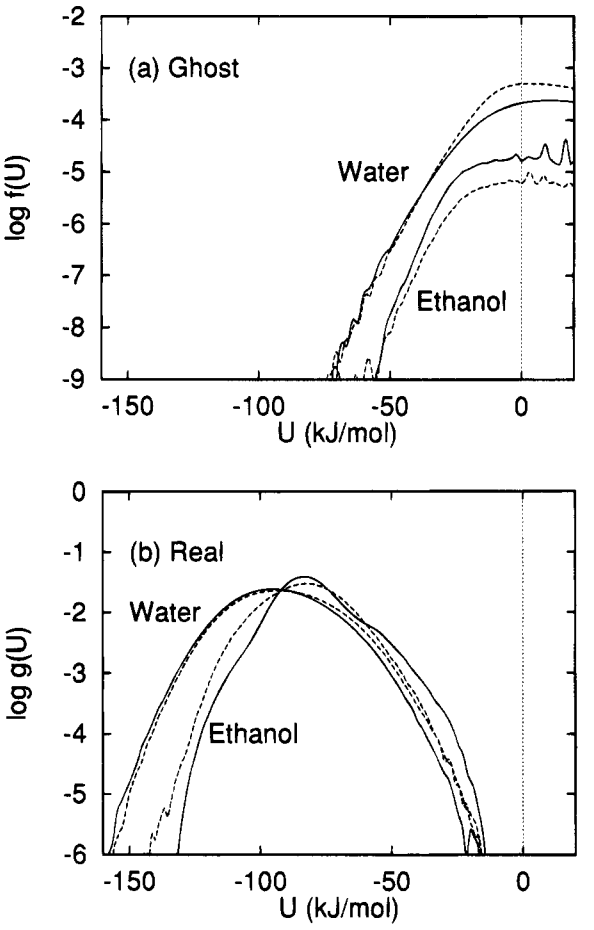

Figure 1. Energy distribution functions (a) $f(U)$ and (b) $g(U)$ of water and ethanol in aqueous ethanol solutions: (solid lines) in the pure liquids (water in water and ethanol in ethanol); (dashed lines) in the 50 wt % solutions.

Although the insertion probability is very low in the insertion of ethanol into the aqueous ethanol solutions, the distribution functions are rather smooth. This shows the advantage of the use of the EVMS and the CCB methods.

In the previous paper,[2] we calculated the insertion probability $P(R)$ of a hard sphere atom into PDMS, PE, water, and ethanol and showed that PDMS had a broader distribution of the free volume than the other systems. In PDMS, the distribution of $f(U)$ has a larger peak than that in any other system. This arises from the broader distribution of free volume. This accounts for the observation that larger molecules are soluble in PDMS.

Since the Lennard-Jones size parameter of water is smaller than that of methane, the $f(U)$ of water in the polymers is larger than that of methane in the high-

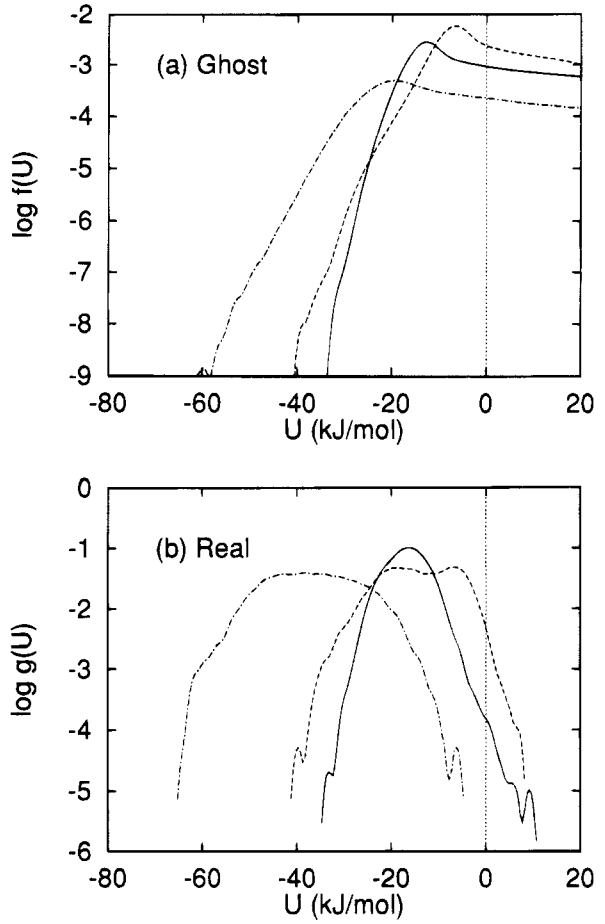

Figure 2. Energy distribution functions (a) $f(U)$ and (b) $g(U)$ of small molecules in PDMS: (solid line) methane; (dashed line) water; (dashed-dotted line) ethanol.

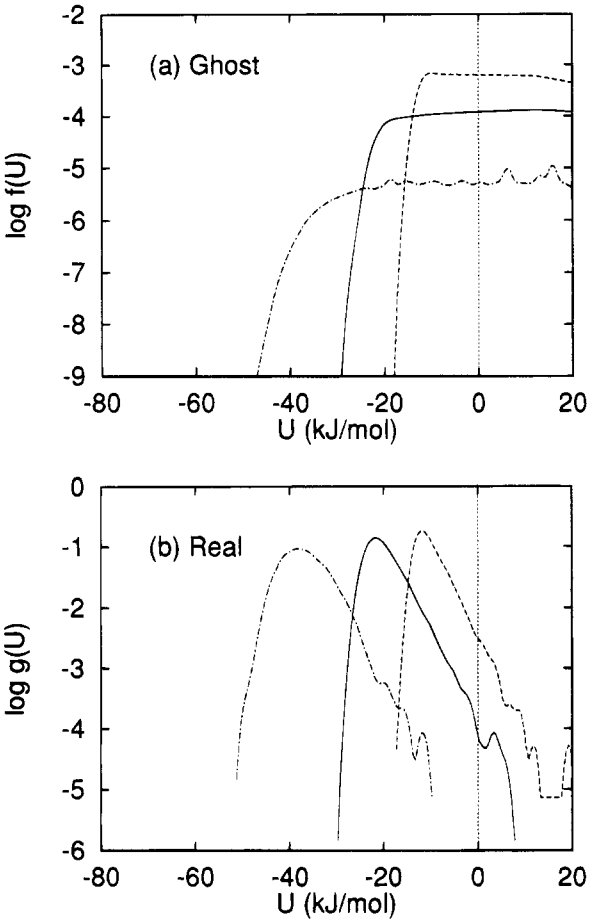

Figure 3. Energy distribution functions (a) $f(U)$ and (b) $g(U)$ of small molecules in PE: (solid line) methane; (dashed line) water; (dashed-dotted line) ethanol.

energy region. Water also has a smaller value of the Lennard-Jones energy parameter. Therefore, in PE, where only the Lennard-Jones term contributes to the interaction, the distribution of the $f(U)$ of methane spreads to the lower energy region whereas that of water is approximately zero below $U = -20$ kJ/mol. The same tendency as in PE is observed in PDMS for $U > -20$ kJ/mol. The difference is found at $U < -20$ kJ/mol; the distribution of the $f(U)$ of water spreads to a lower energy region than methane because of the weak Coulombic interaction. Since ethanol has a larger molecular size than water or methane but a greater Lennard-Jones interaction, the distribution of the $f(U)$ of ethanol is spread to the lower energy region.

There exists a peak in the $f(U)$ of PDMS. In the energy range where the peak in $f(U)$ is found, the ghost molecule feels moderate Lennard-Jones attractive interactions. Therefore, large holes exist in PDMS and the effective insertion trials are attempted mainly in the holes. We will discuss this point in a later subsection.

Using $f(U)$, μ_r is expressed as

$$\mu_r = -kT \ln I(\infty) \tag{19}$$

where

$$I(U) = \int_{-\infty}^{U} f(u) \exp(-u/kT)\, du \tag{20}$$

as plotted in Figure 4. The solid line in Figure 4a shows the $I(U)$ of pure water, and the dashed line shows that of ethanol in the ethanol 50 wt % solutions. For water, half the contribution to $I(U)$ arises from the energy range of $U < -68$ kJ/mol. The low-energy configurations which form the hydrogen-bond contribute significantly to the calculated value of μ_r. The configuration of $U = -78$ and -72 kJ/mol were "incidentally" sampled for ethanol. These two energy points contribute to the main part of $I(U)$. The value of μ_r for ethanol in the 50 wt % solution calculated from eq 19 was -23.7 kJ/mol. (The value is corrected by subtracting the contribution from the dihedral angle potential, as described in a later subsection.) If we ignore the samples with $U = -78$ and -72 kJ/mol, the value of μ_r becomes -13.3 kJ/mol, which is approximately 10 kJ/mol higher than the original value. The probability that a ghost molecule forms hydrogen bonds with the matrix molecules is very low for ethanol. If the hydrogen-bonded configuration is incidentally sampled, the fluctuation of the calculated value becomes large.

Figure 4b shows the plot of $I(U)$ for methane (solid line) and water (dashed line) in PDMS. The profile of $I(U)$ is smooth. Those for all the other polymer/penetrant systems are also smooth, though not shown in the figure. We can expect that the statistical error is very small for these systems. For methane in PDMS, the energy range of $U < -18$ kJ/mol contributes half of $I(U)$. The rest of $I(U)$ arises from the energy ranges of $-18 < U < -8$ kJ/mol, in which the peak in $f(U)$ appears as shown in Figure 2a. For water in PDMS, $I(U)$ tends to increase in lower energy region by the Coulombic interaction and the contribution from $U < -20$ kJ/mol amounts to half of $I(U)$. The peak of $f(U)$ contributes

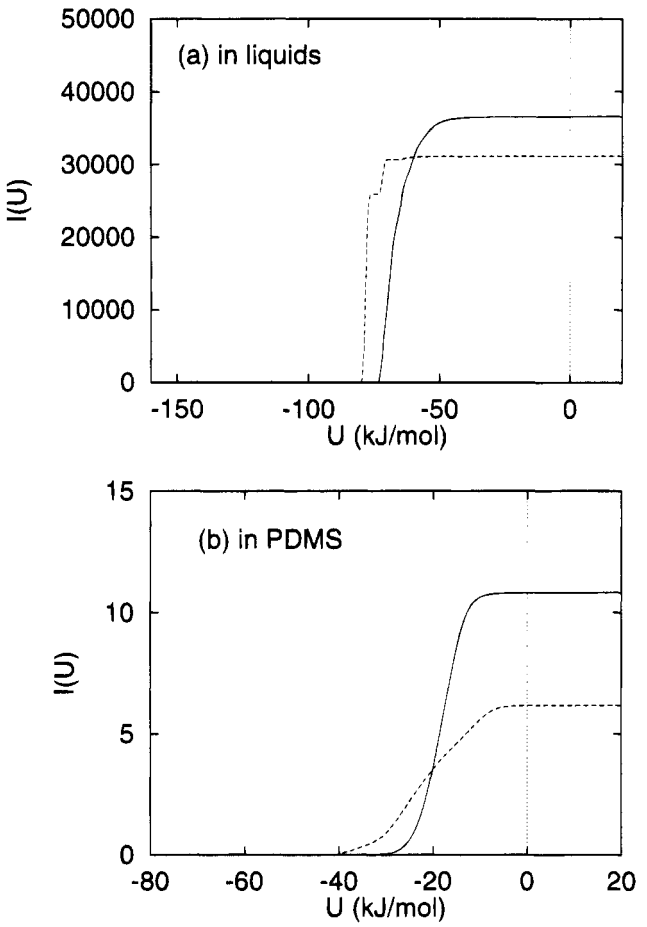

Figure 4. Plots of $I(U) = \int_{-\infty}^{U} f(u) \exp(-u/kT)\, du$ of small molecules: (a) (solid line) water in pure water, (dashed line) ethanol in the 50 wt % aqueous ethanol solution; (b) (solid line) methane in PDMS, (dashed line) water in PDMS.

to a higher energy region than that of methane since the Lennard-Jones interaction is weaker. Therefore, the energy region of $-10 < U < 0$ kJ/mol, in which $f(U)$ has a peak, makes little contribution to the $I(U)$ of water.

The EVMS method affects $f(U)$ at $U > 10$ kJ/mol; $f(U)$ decreases gradually. Since $I(U)$ has saturated fully in this region, the EVMS method can raise the efficiency of sampling without changing the resultant μ_r value.

Real Molecule Energy Distribution Function. The real molecule energy distribution function $g(U)$ was calculated by the inverse-Widom method. Averages were taken for 10 000 coordinates and for the number of molecules for each system. We calculated $g(U)$ for the small molecules in PDMS and in PE using trajectories generated previously.[2] Figure 1b shows $g(U)$ in the aqueous ethanol solutions. Figures 2b and 3b show $g(U)$ in PDMS and in PE, respectively. These figures were obtained from the running average method, as explained for $f(U)$. The distributions in PDMS are broader than in PE. This again arises from the broader distribution of the free volume in PDMS; even the distribution of methane, which has no Coulombic interaction, is broader.

Table 2 lists the components of the interaction energy between the test molecule and the host matrix. The Coulombic interaction is dominant for water and ethanol in the aqueous ethanol solutions. On the other hand, the Lennard-Jones interaction is dominant in PDMS, and the Coulombic interaction makes a minor contribution. In PDMS ethanol interacts with PDMS more strongly than water does.

Table 2. Average Interaction Energy of Real Molecules in kJ/mol

penetrant	LJ	Coulomb	dihedral	total
		In PDMS		
methane	−16.67			−16.67
water	−9.38	−6.09		−15.47
ethanol	−35.59	−4.61	1.99	−38.20
		In PE		
methane	−20.25			−20.25
water	−10.35			−10.35
ethanol	−39.12		2.12	−37.00
		In Pure Water		
water	17.65	−110.68		−93.03
		In 50 wt % Aqueous Ethanol Solution		
water	15.09	−102.93		−87.84
ethanol	−16.31	−66.47	2.02	−80.76
		In Pure Ethanol		
ethanol	−19.96	−62.51	2.06	−80.41

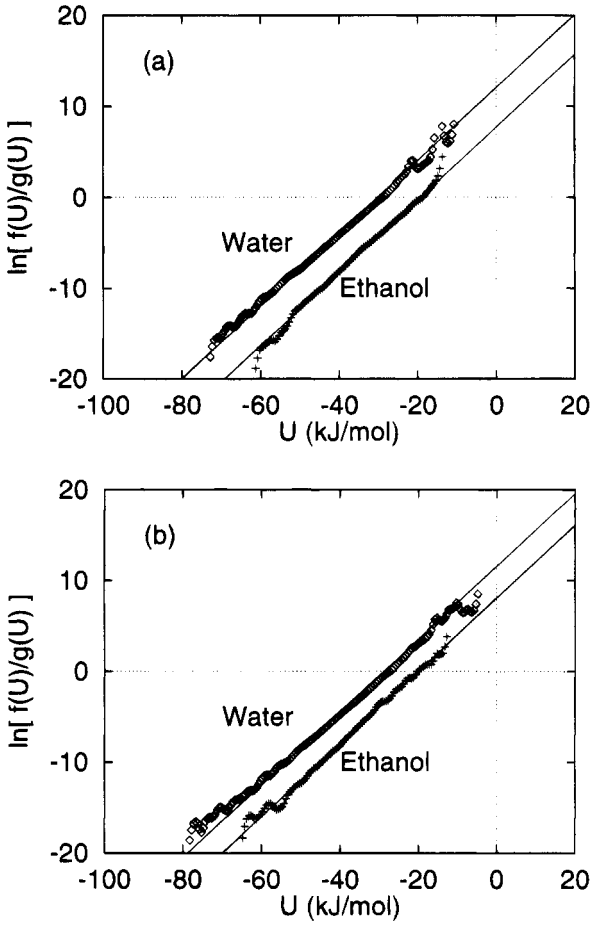

Figure 5. Shing–Gubbins plot for water and ethanol (a) in the pure liquids and (b) in the 50 wt % aqueous ethanol solution. The straight lines show a least-squares fit with the slope fixed to $1/kT$. The intersection with the zero-energy axis is equal to $-\mu_r/kT$.

Shing–Gubbins Plot. We calculated μ_r for the aqueous ethanol solutions by the Shing–Gubbins method. Parts a and b of Figure 5 show the Shing–Gubbins plots for water and ethanol in the pure liquids and in the 50 wt % aqueous ethanol solution, respectively. The straight lines are the least-squares fits with the slope fixed to $1/kT$. The plots show a high linearity and satisfy the condition of a slope of $1/kT$ in the whole energy region. This indicates that the values of μ_r were calculated with a small statistical error.

A Shing–Gubbins plot was made for the small molecules in PDMS and in PE. Straight lines with a

Table 3. Calculated Excess Chemical Potentials in Aqueous Ethanol Solutions Relative to the Ideal Gas Phase

	μ_r (kJ/mol)		
penetrant	0 wt %	50 wt %	100 wt %
	Widom Method[a]		
water	−20.9(2.3)	−23.5(4.0)	
ethanol		−23.5(6.9)	−18.7(4.0)
	Shing−Gubbins Method[b]		
water	−24.9(0.7)	−23.6(1.2)	
ethanol		−18.1(0.2)	−17.2(0.7)

[a] Shown in parentheses are errors which are estimated from 20 subsets of 5 ps each. [b] Shown in parentheses are the differences between the values from least-squares fitting with a slope constrained to $1/kT$ and those from nonconstrained fitting.

slope of $1/kT$ were obtained except for water and ethanol in PDMS, for which $g(U)$ was not accurate enough for evaluation of the chemical potential.

Excess Chemical Potentials. The SPC/E potential function was parametrized so as to include the induced dipole moment effectively.[20] Since the dipole moment of the model is larger than the experimental value in vacuum, the interaction energy is overestimated. Therefore, a polarization correction energy of +5.22 kJ/mol,[20] which is the energy needed for a water molecule to polarize, was added to μ_r for the system of pure water, by assuming that the induced dipole moment was the same on the average for the N molecules system and the $N + 1$ molecules system of a volume V. For water in PDMS, the polarization correction energy is unknown. Because the Coulombic interaction is not dominant in the system, we ignored the polarization correction for this system. The Coulombic interaction energy of water in the 50 wt % solution is not much different from that in pure liquid water, as shown in Table 2. Therefore the magnitude of the induced dipole moment in the aqueous solution is assumed to be the same as that in pure water. Thus, the same correction energy was added for water in the aqueous solution. In the OPLS potential, no induced dipole moment effect is included in the parameter fitting. Therefore, we did not take account of this effect for ethanol.

The free energy of the dihedral angle

$$\mu_{DA} = -kT \ln \int_{-\pi}^{\pi} \exp[-V(\phi)/kT]\, d\phi \qquad (21)$$

was taken into consideration in the reference state of ethanol, where ϕ is the dihedral angle of ethanol and $V(\phi)$ is the torsional potential energy function described by eq 5 in ref 2. The excess chemical potential relative to the ideal gas phase, μ_r, is obtained by subtracting μ_{DA} = −2.03 kJ/mol from the calculated value in the simulation.

Table 3 lists the excess chemical potentials of water and ethanol in the aqueous ethanol solutions. The chemical potential values were also calculated for the *NPT* ensemble according to eq 3. For the *NPT* ensemble these agree within 0.03 kJ/mol with those for the *NVT* ensemble. Since the fluctuation of the volume is very small in a usual liquid, eq 3 has no advantage in this case.

Errors for the Widom method are estimated as standard deviations of 20 separate subsets of 5 ps each. Each subset is composed of 500 configurations. Errors in the Shing−Gubbins method are estimated as the differences between two chemical potential from least-squares fitting with a slope constrained to $1/kT$ and from nonconstrained fitting. Comparing the result from the Widom method with that from the Shing−Gubbins method, we find that agreement in the Widom and the Shing−Gubbins methods is excellent for water in the 50 wt % aqueous ethanol solution. For water in pure water and for ethanol in the aqueous solutions, however, agreement is rather poor. In the Widom method, the probability that the ghost molecule forms hydrogen bonds with the matrix molecules is very low. If the hydrogen-bonded configuration is incidentally sampled, the fluctuation of the calculated value becomes large. On the other hand, stable hydrogen-bonded configurations are almost always sampled in the inverse-Widom method. Since use of both $f(U)$ and $g(U)$ has the benefit of a mutual error cancelation in the Shing−Gubbins method, we can expect that the statistical error is small even for ethanol. This is indeed true, as shown in Table 3. Therefore, the chemical potential values from the Shing−Gubbins method are used in the following analysis.

Table 4. Calculated Excess Chemical Potentials in Polymers Relative to the Ideal Gas Phase

	μ_r (kJ/mol)	
penetrant	in PDMS	in PE
	Widom Method[a]	
methane	−5.84(0.12)	−1.17(0.58)
water	−4.44(0.40)	2.99(0.21)
ethanol	−15.5(1.2)	−6.1(1.5)
	Shing−Gubbins Method[b]	
methane	−5.3(0.5)	−1.0(1.3)
water		2.9(2.8)
ethanol		−6.0(1.4)

[a] Shown in parentheses are errors which are estimated from 10 subsets of 50 ps each. [b] See footnote *b* of Table 3.

The calculated excess chemical potential of liquid water is slightly lower than the experimental value −23.9 kJ/mol.[29] The excess free energy of mixing of the 50 wt % aqueous ethanol solution was estimated to be a positive value, 0.7 kJ/mol, which agrees reasonably with the experimental value, ~0.5 kJ/mol.[30] This shows the adequacy of our simulation.

In our previous paper,[3] we performed MD simulations for pure water (216 molecules) and for pure ethanol (128 molecules) under constant *NVT* conditions and calculated μ_r by the Widom method. The chemical potentials for water and ethanol were −27.5(5.0) and −8.9(2.8) kJ/mol, respectively (errors are in parentheses). The chemical potential of water is lower than that in the present simulation by 2.6 kJ/mol, and that of ethanol is higher by 8.3 kJ/mol. One reason for the discrepancy is that the "incidentally" sampled low-energy configuration makes a large contribution to the value of μ_r in the Widom method. To overcome this, a Shing−Gubbins plot was also made for the system of the *NVT* ensemble. The chemical potentials for water and ethanol are −25.5(3.0) and −12.0(2.7) kJ/mol, respectively, which are closer to those of the *NPT* ensemble by the same method than those by the Widom method. For ethanol, however, the difference is approximately 5 kJ/mol. The density is approximately 4% lower in the *NPT* ensemble than in the *NVT* ensemble. This leads to a difference in the average values of the accessible volume fraction for an oxygen atom of ethanol: 0.055 in the *NPT* ensemble and 0.038 in the *NVT* ensemble. This is supposed to be one of the origins for the difference in μ_r.

Table 4 lists μ_r of the small molecules in the polymers. The error was estimated in the same way as in the case

Table 5. Calculated Solubilities in PDMS and PE at 300 K[a]

penetrant	polymer	S_g	S_l 0 wt %	S_l 50 wt %	S_l 100 wt %
methane	PDMS	10.4(0.5)			
water	PDMS	5.9(1.0)	$2.76(0.82) \times 10^{-4}$	$4.6(2.3) \times 10^{-4}$	
ethanol	PDMS	490(250)		$3.5(1.8) \times 10^{-1}$	$5.0(2.6) \times 10^{-1}$
methane	PE	1.60(0.38)			
water	PE	0.302(0.025)	$1.40(0.42) \times 10^{-5}$	$2.3(1.2) \times 10^{-5}$	
ethanol	PE	11.6(7.2)		$8.3(5.1) \times 10^{-3}$	$11.8(7.3) \times 10^{-3}$

[a] Errors are in parentheses.

Table 6. Calculated Permeation Rates in PDMS and PE at 300 K

penetrant	polymer	P_g (cm²/s)	P_l (cm²/s) 0 wt %	P_l (cm²/s) 50 wt %	P_l (cm²/s) 100 wt %
methane	PDMS	5.9×10^{-5}			
water	PDMS	9.1×10^{-5}	4.2×10^{-9}	7.0×10^{-9}	
ethanol	PDMS	9.8×10^{-4}		7.0×10^{-7}	10.0×10^{-7}
methane	PE	2.6×10^{-6}			
water	PE	2.4×10^{-6}	1.1×10^{-10}	1.8×10^{-10}	
ethanol	PE	8.1×10^{-6}		5.8×10^{-9}	8.3×10^{-9}

of aqueous ethanol solutions; all of the configurations are separated into 10 subsets each of which consists of 100 configurations corresponding to a 50 ps trajectory. The values of μ_r from the Widom method agree well with those from the Shing–Gubbins method. For the systems of water and ethanol in PDMS, the Shing–Gubbins plots were not linear. The small molecules diffuse by the jump process in the polymers; the vibrational motion in a cage is dominant for most of the simulation time. It is difficult to sample all the configurational space during the simulation time. Therefore, $g(U)$ is liable to have some statistical errors. On the other hand, the Widom method does not suffer from such a problem. Since the Lennard-Jones interaction is dominant in PDMS and PE, the errors which are caused mainly by the strong Coulombic interaction are expected to be very low. The estimated errors in Table 4 support this conjecture. Therefore, we use the μ_r from the Widom method for the small molecules in the polymers.

The chemical potentials are always lower in PDMS than in PE. This is due to the broader free volume distribution in PDMS. The ethanol molecule is larger in size but has a lower μ_r than water or methane because the Lennard-Jones interaction is stronger.

Solubility of Penetrant in Polymer. The solubilities, S_g and S_l, were calculated from eqs 11 and 12, respectively, and are listed in Table 5. The solubility of methane in PDMS is higher than the experimental value 0.56[7] but is close to the calculated value 12.5 by Sok et al.[7] using the Widom method. Since the standard deviation is very small, the discrepancy with the experimental value is probably due to inaccuracy of the potential functions. The solubilities, S_l, of ethanol are approximately 760 and 350 times higher in PDMS and PE, respectively, than those of water. Although the insertion probability of ethanol in PDMS is smaller than that of water, the solubility of ethanol is higher than that of water because the Lennard-Jones interaction of ethanol is stronger. The solubilities, S_g, of methane, water, and ethanol in PDMS are approximately 7, 20, and 42 times higher, respectively, than those in PE. This is due to the broader free volume distribution in PDMS. For a large molecule such as ethanol, the difference in solubility is significant.

Okamoto et al.[31] measured the solubilities of the aqueous solution of ethanol at various concentrations by sorption experiments. Water has a low solubility in the PDMS membrane, and there are no experimental data for pure liquid water. The solubility extrapolated to zero concentration of ethanol is smaller than 1×10^{-3}. The calculated solubility, 2.76×10^{-4}, agrees reasonably well with the experiment. The solubility of liquid ethanol, 0.50, is higher than the experimental value, 0.092. The solubilities at infinite dilution were calculated in this simulation. Considering the fact that the deviation from Henry's law becomes larger for a penetrant with high solubility, the agreement between the calculated and experimental values is satisfactory.

Permeation Rate. In our previous paper[2] the diffusion coefficients D were determined for small molecules in polymers. The diffusion coefficients for methane, water, and ethanol in PDMS are 0.57×10^{-5}, 1.53×10^{-5}, and 0.20×10^{-5} cm²/s, respectively, and those in PE are 0.16×10^{-5}, 0.78×10^{-5}, and 0.07×10^{-5} cm²/s. Ethanol, which is larger in size than water, has a smaller diffusion coefficient in polymers than water.

The permeation rate was calculated from the product of the diffusion coefficient and the solubility and is listed in Table 6. P_g and P_l were calculated from S_g and S_l. Considering the accuracy of simulations and experiment, our calculated values agree with the experimental values: 1.1×10^{-5}, $<1 \times 10^{-8}$, and 4.1×10^{-7} cm²/s for methane gas, pure liquid water, and pure liquid ethanol in PDMS at 300 K.[31,32] The agreement between the simulation and the experiments is better than in our previous paper.[3] This is probably due to the use of the Shing–Gubbins method for the calculation of the excess chemical potentials in the liquids. The result that the permeation rate of ethanol is higher than water agrees with the permselectivity of ethanol by the PDMS membrane. Ethanol has a smaller diffusion coefficient than water in PDMS but has a much larger permeation rate. This is a consequence of the difference in solubility between water and ethanol.

Cluster Analysis of Free Volume. Figure 4 in ref 2 shows the broader distribution of the insertion probability $P(R)$ of hard sphere atoms of radius R in PDMS. Therefore, a large solubility is expected even for a relatively large molecule in PDMS.

To obtain further information about the free volume, we performed a cluster analysis of the free volume using a water molecule (radius 1.5828 Å) as a probe. Parts a and b of Figure 6 show the accessible volume clusters

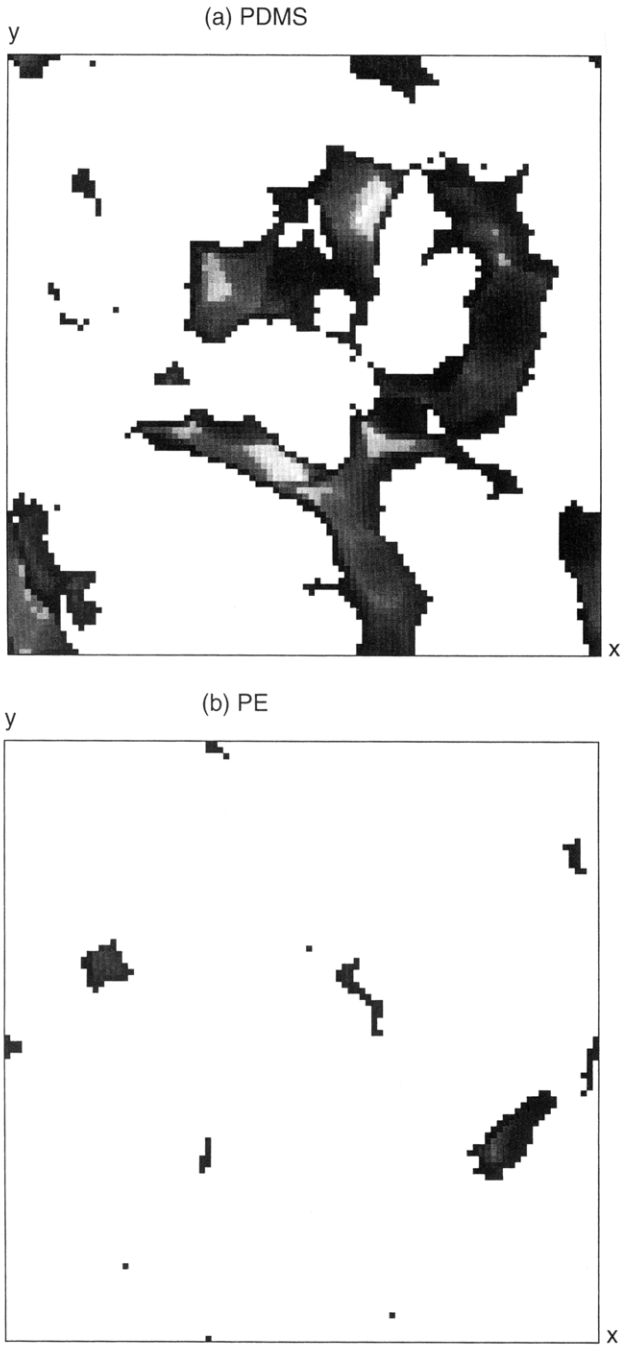

Figure 6. The $x-y$ projections of accessible clusters (a) in PDMS and (b) in PE, using a water molecule as a probe.

in the instantaneous configuration of PDMS and of PE, respectively. The figures show the projection of the unit cells onto the $x-y$ plane. The cell lengths are 27.24 and 25.46 Å for PDMS and PE, respectively. The white parts in the background indicate the regions in which the overlaps between water and the polymers are severe. The accessible clusters are expressed by gray-scale. The brighter the grid point in the cluster is, the more accessible cubes exist in the depth direction. Therefore, the central region of the large cluster is white. The free volume clusters in PDMS are larger than those in PE. Note that the figures are projections of the clusters onto the planes. The cluster looks larger than a real cluster. The channel through which a small penetrant permeates is narrow. The free volume fractions with a water molecule as a probe were approximately 1.8% for PDMS and 0.05% for PE.

Table 7. Cluster Analysis of Accessible Cubes for Water

matrix	$10^4 f_v$	$\langle V_c \rangle$ (Å^3)	$\langle s^2 \rangle^{1/2}$ (Å)	$\langle b/s^2 \rangle$
Accessible Clusters in Polymers				
PDMS	176.7	166.67	6.15	0.567
PE	5.0	6.54	1.32	0.542
Accessible Clusters in Liquids				
0 wt %[a]	0.7	0.65	0.58	0.552
50 wt %[a]	7.0	11.48	1.97	0.570
100 wt %[a]	10.4	8.18	1.37	0.520

[a] Concentration of the aqueous ethanol solution.

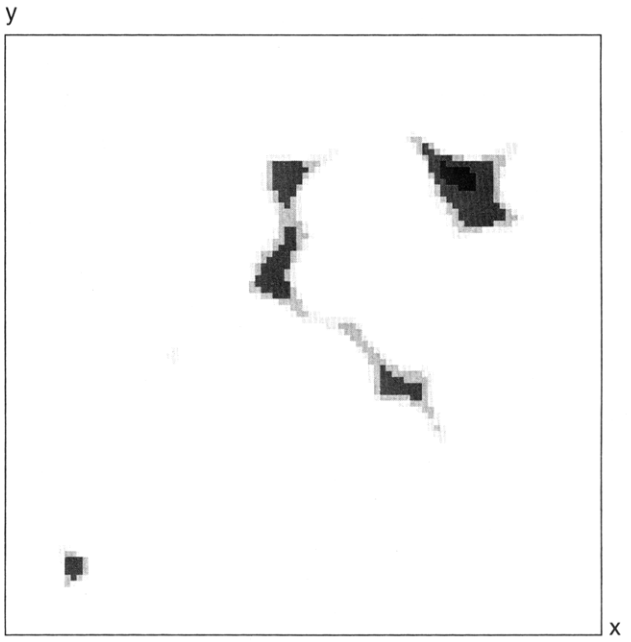

Figure 7. Energy map for a methane molecule in PDMS on an arbitrarily chosen plane parallel to the $x-y$ plane. The energies are divided into five regions between $U = -18$, -8, 0, and 10 kJ/mol; the lower energy region is painted darker.

Table 7 lists the free volume fraction f_v, the average volume of the clusters $\langle V_c \rangle$, the root mean-square radius of gyration $\langle s^2 \rangle^{1/2}$, and the asphericity $\langle b/s^2 \rangle$. The value f_v is an arithmetic mean over 100 coordinates, and the other values are the averages weighted by the volume of the clusters. The value of f_v is larger in PDMS than in the other systems. The values of $\langle V_c \rangle$ and $\langle s^2 \rangle^{1/2}$ are also large in PDMS. The radius of gyration of clusters in PDMS, 6.15 Å, is sufficiently large compared with the kinetic radius of ethanol, 2.604 Å.[33] This does not mean that a cavity with a radius of 6 Å exists in the polymer matrix but means that cavities which are connected by channels are spread over an area with a radius of 6 Å. This structure of the free volume in PDMS leads to the large diffusion coefficients of small penetrants in PDMS, and the fact that larger molecules are soluble in PDMS. For the asphericity, no marked difference is found among the systems.

Energy Map of Ghost Molecule. A three-dimensional energy map of the ghost molecule was generated to examine where the effective sampling points are distributed in the unit cell. Considering 100 × 100 × 100 grid points in the unit cell of PDMS, all the grid points were classified by the interaction energy U between a methane molecule on the grid point and the host matrix. Figure 7 shows the energy map for a methane molecule in PDMS on an arbitrarily chosen plane parallel to $x-y$. The energies are divided into five classes separated at $U = -18$, -8, 0, and 10 kJ/mol. The darkest region in the figure shows the most stable

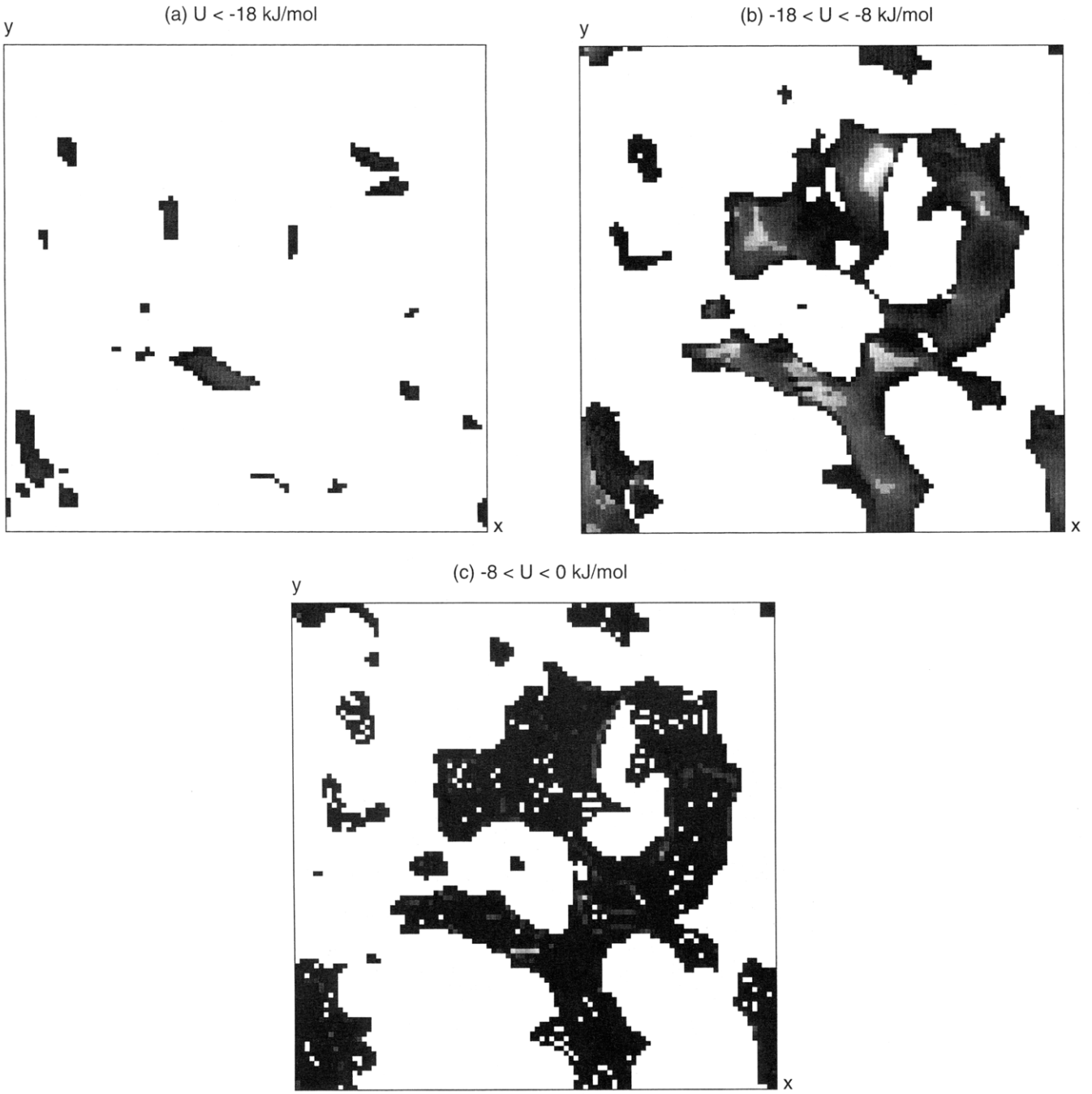

Figure 8. The $x-y$ projections of the clusters of grid points at which a methane molecule interacts with the surrounding matrix of PDMS in the energy ranges (a) $U < -18$, (b) $-18 < U < -8$, and (c) $-8 < U < 0$ kJ/mol.

region: $U < -18$ kJ/mol. The white region shows the unstable region: $U > 10$ kJ/mol. The middle energy regions were painted by grayscale. The low-energy regions look like islands surrounded by higher energy regions. The dark regions of the figure correspond to the channels through which a methane molecule can permeate with low energy.

The cluster analysis was performed for grid points which belong to the same class. Parts a–c of Figure 8 show the projection of the clusters with $U < -18$, $-18 < U < -8$, and $-8 < U < 0$ kJ/mol, respectively. Table 8 lists the results of the cluster analysis. Figure 8a shows the low-energy regions at which U is less than -18 kJ/mol. The regions are surrounded by the clusters of $-18 < U < -8$ kJ/mol, which are shown in Figure 8b. The lower energy regions are not restricted to a small area but rather are scattered uniformly. The clusters move ubiquitously in the cell as time evolves.

Table 8. Cluster Analysis of Energy Map for Methane in PDMS

U (kJ/mol)	$10^4 f_v$	$\langle V_c \rangle$ (Å^3)	$\langle s^2 \rangle^{1/2}$ (Å)	$\langle b/s^2 \rangle$
$U < -18$	13.5	3.55	0.98	0.523
$-18 < U < -8$	203.5	186.97	6.78	0.575
$-8 < U < 0$	87.4	4.72	1.96	0.616

Therefore, the points where the low-energy configurations are sampled are randomly distributed in the unit cell. Referring to Figure 4, these regions contribute half to $I(U)$, in spite of the small volume.

Figure 8b shows the region $-18 < U < -8$ kJ/mol, which contributes to the peak in $f(U)$ of methane in PDMS, as shown in Figure 2a. The size and position of the clusters correspond to the free volume clusters in Figure 6a. Comparing Table 7 with Table 8 shows that each item of the clusters of the energy map for $-18 < U < -8$ kJ/mol agrees well with that of the free

volume in PDMS (the former is slightly larger). Therefore, the peak in $f(U)$ is attributed to the insertion trials into the large free volume. The radius of water, 1.5828 Å, is approximately 85% of that of methane (1.865 Å). Many effective samplings were made for the regions which are accessible for a probe with a radius of 85% of the molecular radius. When the excluded volume map is generated in the EVMS method, the Lennard-Jones size parameters of both a matrix atom and a test atom are scaled by the factor a in eq 4. Therefore the white background in Figure 6a corresponds to the excluded volume map of methane with a scale factor of $a = 0.92$.

Figure 8c shows the energy region of $-8 < U < 0$ kJ/mol. The clusters are spread widely in the entire cell. The dark black grid points show that the depths of all the clusters are small. By comparison of each item in Table 8, f_v is 43% of that of $-18 < U < -8$ kJ/mol. Nevertheless, $\langle V_c \rangle$ is only 2.5%. The region $-8 < U < 0$ kJ/mol in Figure 8c surrounds the region $-18 < U < -8$ kJ/mol in Figure 8b. The former region, however, makes little contribution to $I(U)$, as shown in Figure 4.

Conclusions

The excess chemical potentials μ_r of methane, water, and ethanol in PDMS and PE were calculated by the Widom method. The excess chemical potentials of water and ethanol in the aqueous ethanol solutions (0, 50, 100 wt %) were also calculated by the Shing–Gubbins method. The solubilities of the small molecules in the polymers were calculated from the values of μ_r.

PDMS and PE are hydrophobic polymers. The solubility of ethanol is much larger than that of water in PDMS and PE. This is owing to the Lennard-Jones interaction between ethanol and the polymers. The free volume analysis shows that PDMS has larger free volume clusters than the other systems. PDMS has a structure in which a large molecule is soluble.

The permeation rates, which were calculated from the diffusion coefficients and the solubilities, were in reasonable agreement with experimental data. Although ethanol has a smaller diffusion coefficient than water, ethanol has a larger permeation rate. This is because ethanol has a higher solubility in PDMS. This character explains the ethanol selectivity of the PDMS membrane.

Acknowledgment. The authors thank J. K. Button for a critical reading of the manuscript. Generous amounts of computer time were provided by the Supercomputer Laboratory, Institute for Chemical Research, Kyoto University. Computer time was provided also by the Computer Center, Institute for Molecular Science. This work was supported in part by Tosoh Corp., Japan.

References and Notes

(1) Huang, R. Y. M., Ed. *Pervaporation Membrane Separation Processes*; Elsevier Science Publishers B. V.; Amsterdam, The Netherlands, 1991.
(2) Tamai, Y.; Tanaka, H.; Nakanishi, K. *Macromolecules* **1994**, *27*, 4498.
(3) Tamai, Y.; Tanaka, H.; Nakanishi, K. *Fluid Phase Equil.*, in press.
(4) Widom, B. *J. Chem. Phys.* **1963**, *39*, 2808.
(5) Panagiotopoulos, A. *Z. Mol. Simul.* **1992**, *9*, 1.
(6) Müller-Plathe, F. *Macromolecules* **1991**, *24*, 6475.
(7) Sok, R. M.; Berendsen, H. J. C.; van Gunsteren, W. F. *J. Chem. Phys.* **1992**, *96*, 4699.
(8) Müller-Plathe, F.; Rogers, S. C.; van Gunsteren, W. F. *J. Chem. Phys.* **1993**, *98*, 9895.
(9) Gusev, A. A.; Suter, U. W. *J. Chem. Phys.* **1993**, *99*, 2228.
(10) Deitrick, G. L.; Scriven, L. E.; Davis, H. T. *J. Chem. Phys.* **1989**, *90*, 2370.
(11) Cracknell, R. F.; Nicholson, D.; Parsonage, N. G.; Evans, H. *Mol. Phys.* **1990**, *71*, 931.
(12) de Pablo, J. J.; Laso, M.; Suter, U. W. *J. Chem. Phys.* **1992**, *96*, 6157.
(13) Laso, M.; de Pablo, J. J.; Suter, U. W. *J. Chem. Phys.* **1992**, *97*, 2817.
(14) Kumar, S. K.; Szleifer, I.; Panagiotopoulos, A. *Z. Phys. Rev. Lett.* **1991**, *66*, 2935.
(15) Sheng, Y. J.; Panagiotopoulos, A. Z.; Kumar, S. K.; Szleifer, I. *Macromolecules* **1994**, *27*, 400.
(16) Kumar, S. K. *Macromolecules* **1994**, *27*, 260.
(17) Shing, K. S.; Gubbins, K. E. *Mol. Phys.* **1982**, *46*, 1109.
(18) Gubbins, K. E. *Mol. Simul.* **1989**, *2*, 223.
(19) Jorgensen, W. L.; Tirado-Rives, J. *J. Am. Chem. Soc.* **1988**, *110*, 1657.
(20) Berendsen, H. J. C.; Grigera, J. R.; Straatsma, T. P. *J. Phys. Chem.* **1987**, *91*, 6269.
(21) Nosé, S. *J. Chem. Phys.* **1984**, *81*, 511.
(22) Andersen, H. C. *J. Chem. Phys.* **1980**, *72*, 2384.
(23) Ferrario, M.; Ryckaert, J. P. *Mol. Phys.* **1985**, *54*, 587.
(24) Allen, M. P.; Tildesley, D. J. *Computer Simulation of Liquids*; Oxford University Press: Oxford, U.K., 1987; p 64.
(25) Arizzi, S.; Mott, P. H.; Suter, U. W. *J. Polym. Sci., Polym. Phys. Ed.* **1992**, *30*, 415.
(26) Greenfield, M. L.; Theodorou, D. N. *Macromolecules* **1993**, *26*, 5461.
(27) Misra, S.; Mattice, W. L. *Macromolecules* **1993**, *26*, 7274.
(28) Jorgensen, W. L. *J. Phys. Chem.* **1986**, *90*, 1276.
(29) Sarkisov, G. H.; Dashevsky, V. G.; Malenkov, G. G. *Mol. Phys.* **1974**, *27*, 1249.
(30) Mulder, M. H. V.; Smolders, C. A. *J. Membr. Sci.* **1984**, *17*, 289.
(31) Okamoto, K.; Nishioka, S.; Tsuru, S.; Sasaki, S.; Tanaka, K.; Kita, H. *Kobunshi Ronbunshu* **1988**, *45*, 993.
(32) Stern, S. A.; Shah, V. M.; Hardy, B. J. *J. Polym. Sci., Polym. Phys. Ed.* **1987**, *25*, 1263.
(33) Loyd, D. R.; Meluch, T. B. *ACS Symp. Ser.* **1985**, *269*, 47.

MA9450501